RESEARCH PAPER

Waviness-induced passive particle manipulation of very dilute suspensions in confined microfluidic flows

Abner Luna Garcia[1] · Javed Akhtar[1] · Leonardo Saenz[1] · Fangjun Shu[1] · Sarada Kuravi[1] · Krishna Kota[1]

Abstract

This study reports a new observation of rapid particle migration in very dilute suspensions flowing through a microchannel. In microfluidics, passive particle manipulation methods based on shear gradients or inertial forces are usually preferred from an energy consumption perspective. Shear-induced migration is known to be particularly slow (requires very long channels) compared to inertial migration. In this case, neutrally buoyant particles usually follow the fluid flow field and could migrate laterally to the flow toward the center, i.e., in the direction of decreasing shear stress. This migration was experimentally observed for dense colloids and suspension flows with high particle concentrations, generally exceeding 25%. However, achieving this migration passively in very dilute suspensions is challenging, typically resulting in the same concentration distribution at the inlet, along the length, and at the microchannel outlet. In this effort, two-dimensional waviness was assigned to the walls of a confined microchannel, and flow visualization was employed to study whether this passive approach has the potential to move the particles toward walls in a very dilute suspension (0.1% concentration) for flow Reynolds numbers < 100 (in the realm of microfluidics). The approach was tested for two different particle sizes (2 µm and 6 µm) and two flow rates in a pressure-driven flow configuration. The results of particle counting from the captured images showed that wall waviness creates an asymmetric velocity profile for the fluid where the maximum velocity alternately moves closer to the wave peaks or crests on both the channel walls vs. a symmetric parabolic profile in a straight-walled channel. This asymmetry moved the particles toward the wavy walls (closer to the wave crests), where the shear stress was minimum. Even with a highly conservative estimation, it was observed that this migration or settling of the particles into two streams—one near each wall—for the wavy microchannel started to occur at an effective flow length that is less than 10% of the theoretical length required for the particles to migrate to an equilibrium position in a straight microchannel. Remarkably, this waviness-induced particle manipulation was achieved without generating turbulence or secondary flows (no Dean vortices) and, therefore, will markedly assist in controlling the pressure drop increase.

1 Introduction

The ability to manipulate particles in suspension flows can be a powerful tool for realizing numerous compact microfluidic systems with desired functionality. Therefore, controlled manipulation or focusing of synthetic and biological particles, e.g., cells, pathogens, and drugs, is a topic of great interest. It has a vast array of small and large-scale applications such as particle separation or cell separation (Guan et al. 2013; Alshareef et al. 2013; Bhagat et al. 2010),

particle filtration (Gallager 1988; Wang et al. 2012), desalination (Ren and Liang 2020; Said et al. 2020), water and slurry transportation, thermal management (Kuravi et al. 2009), biomedical and biochemical research (Ateya et al. 2008; Nilsson et al. 2009; Karimi et al. 2013), drug discovery and delivery systems (Kang et al. 2008; Nguyen et al. 2013), disease diagnostics and therapeutics (Suresh et al. 2005; Vaziri and Gopinath 2008), and self-cleaning and antifouling technologies (Callow and Callow 2011; Nir and Reches 2016).

Particles in microchannel flows can be manipulated by taking advantage of either internal or external forces. The corresponding methods can be categorized based on their working principle, such as hydrodynamic (Li et al. 2013; Liu and Hu 2017; Xie et al. 2018), acoustic (Hardt and Schönfeld 2007; Kiyasatfar and Nama 2018), electrical (Esseling

✉ Krishna Kota
kkota@nmsu.edu

1 Department of Mechanical and Aerospace Engineering, New Mexico State University (NMSU), Las Cruces, NM 88003, USA

et al. 2012; Kumar et al. 2020), optical (Jonáš and Zemanek 2008; Conkey et al. 2011; Varanakkottu et al. 2013; Paiè et al. 2018), magnetic (Mirowski et al. 2004; Niu et al. 2014), etc. Of these, hydrodynamic manipulation is a passive internal phenomenon based on the balance of the fluidic forces that cause migration of the particles to an equilibrium position and involves no additional energy consumption, is a relatively simple setup, and is independent of external force fields.

Hydrodynamic migration of particles inside a microchannel is a function of the particle type, size, shape, volume fraction, fluid type, and channel wall geometry or curvature. By adjusting these variables, migration can be controlled reasonably and classified as either inertial or shear-induced type. Inertial migration occurs in flows with a particle Reynolds number > 1. Here, particles move laterally orthogonal to the flow direction to an equilibrium position where the inertial drag and the inertial lift forces acting on them are balanced. Inertial microfluidics is an active field of study, considering it has various applications (e.g., Lee et al. 2011; Zhang et al. 2020; Segre and Silberberg 1962; Gao 2017; Martel and Toner 2014)).

On the other hand, shear-induced particle migration was also extensively studied in the literature and was initially observed by Karnis et al. (Karnis, 2, Goldsmith, H.L. and Mason, S.G. 1966). Numerical and experimental studies and phenomenological models (such as diffusive flux model and suspension balance model) have shown that particles migrate across the streamlines in pressure-driven flows. This migration was found to occur from the high-shear region near the walls to the low-shear region at the center of flow channels, e.g., refs. (Gadala-Maria and Acrivos 1980; Hampton et al. 1997; Koh et al. 1994; Leighton and Acrivos 1987; Phillips et al. 1992; Nott and Brady 1994). Researchers also found that the normal stress on the particles generates the driving force required for their migration (Boyer et al. 2011; Morris and Boulay 1999; Dbouk and Habchi 2019). However, compared to inertial migration, shear-induced migration is a prolonged process requiring long channels. It was found to happen mainly in dense suspension flows (volume concentration > 25%) with a particle Reynolds number < 1 (Karnis et al. 1966; Gadala-Maria and Acrivos 1980; Hampton et al. 1997; Koh et al. 1994; Leighton and Acrivos 1987; Phillips et al. 1992; Nott and Brady 1994; Boyer et al. 2011; Morris and Boulay 1999; Dbouk and Habchi 2019).

Shear-induced migration of dilute suspensions has applications in particle separation, filtration, counting, detecting, sorting, or mixing in the food industry, coating industry, biological flows, material processing operations, medicine, petroleum industry, cosmetics and paints, injection molding, characterization of magnetic and ferrofluids, and thermal management of electronics (e.g., Yadav et al. 2015; Davis 2019; Schroen et al. 2017; Dontsov et al. 2019; Goris and

Osswald 2018; Hong et al. 2004; Rebouças et al. 2018; Siqueira et al. 2017a; Siqueira and Carvalho 2019; Cunha et al. 2016; Fan et al. 2003; Petrie 1999; Tripathi and Bég 2014; Klaver and Schroën 2015; Kuravi 2009)). However, despite its utility, it is challenging to achieve in very dilute suspensions, which generally results in the same concentration distribution at the inlet, along the length, and at the microchannel outlet (Carlo et al. 2007).

This study aims to pursue a passive approach for manipulating particles of very dilute suspensions (0.1% concentration) flowing through a microchannel. It is based on engineering the channel wall geometry to favor a relatively rapid migration of particles to specific locations in the channel for easy separation, sorting, or detection. Toward this goal, sinusoidal waviness with an amplitude-to-wavelength ratio of 0.2 was assigned to the microchannel walls. Wavy channels were previously studied in a few microfluidics applications, primarily for mixing using secondary flows (Bhagat et al. 2010; Solehati et al. 2018; Zhou et al. 2018). However, they were not explored, especially from the point of view of particle manipulation of dilute suspensions. The velocity profile in a wavy microchannel was obtained using micro-particle image velocimetry (μ-PIV), and its effect on manipulating the particle concentration profile is discussed.

2 Methodology

A μ-PIV setup was used for particle visualization experiments. A schematic of this setup is shown in Fig. 1. It comprises an inverted microscope (Olympus IX73), an Nd:YAG dual-head pulse laser with a wavelength of 532 nm, an external synchronizer, a charge-coupled device (CCD) camera, and a computer with DaVis 8.2 software installed for PIV analysis. The microscope was used to magnify the frame by 20 times to focus the microscopic-sized particles in better resolution. A temporal resolution of 3 Hz was used for image acquisition, and 400 pairs of images were secured for each
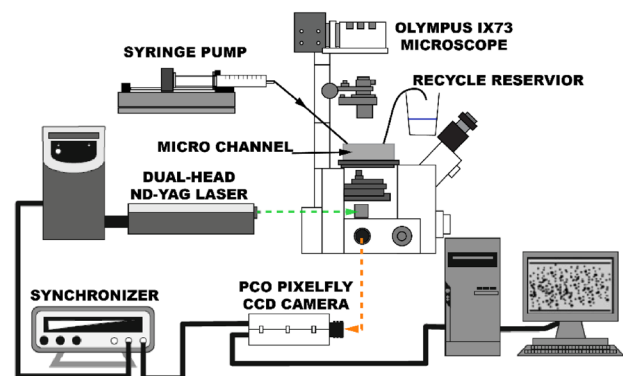

Fig. 1 Schematic of the μ-PIV flow visualization setup

scenario of the experiment to capture and count the particle distribution in the microchannel.

A syringe pump was used to drive the flow in the setup since it provided a constant mean fluid flow rate throughout the experiment. Fluorescent particles of 2 µm and 6 µm were used to study their migration characteristics. For obtaining the velocity profiles, 500 nm seeding particles were used. All the particles have a refractive index of 1.59 at 589 nm, an excitation peak at 542 nm, and an emission peak at 612 nm.

A straight-walled channel with a width of 200 µm (W), 80 µm of height (H) or depth, and 6 cm of length (L) was used in the experiments. Based on the fabrication feasibility provided by the available resources, a 300 µm-wide sinusoidal wavy-walled microchannel (Eq. (1)) of the same height and length as the straight channel with a wavelength (λ) of 400 µm and an amplitude (A) of 80 µm for the walls was prepared for studying the channel wall geometry effect on particle migration.

$$y = A \cdot \sin\left(\frac{2\pi}{\lambda}x\right) \tag{1}$$

where x and y are the flow and lateral directions coordinates, respectively.

The migration phenomenon was studied along the width for both the straight and the wavy-walled microchannels, considering it is the cross-section's more challenging (i.e., larger) dimension. The channels were fabricated by uFluidix (https://www.ufluidix.com/) in polydimethylsiloxane (PDMS) in four stages: preparing the negative master (mold), pouring PDMS into the mold, detaching PDMS from the mold, and bonding PDMS to a glass slide.

The particle suspension was loaded into a 3 ml syringe and placed in a syringe pump set to maintain the desired flow rate. The syringe was attached to one end of a 2 mm diameter transparent plastic tube using a Luer lock fitting, and the other end of the tube was connected to the inlet port of the microchannel with a barbed tube fitting. Another barbed tube fitting was used to connect the exhaust tube to the outlet port that leads to a recycle reservoir to reuse the particle suspension. The tubes used for the inlet and outlet were semi-rigid and not overly long to avoid increased pressure drop in the setup. Figure 2 shows the schematics and the fabricated microchannels used in the experiments.

Particle volume concentrations of around 0.1% were used to simulate a very dilute suspension. The density of the particles (1050 kg/m³) is almost the same as the density of the base fluid (water) used, and therefore, they were assumed to remain neutrally buoyant in the mixture. Additionally, trace amounts of a surfactant were added to the mixture to prevent the agglomeration of particles in the suspension. Finally, the suspension was stirred adequately with a magnetic stirrer for two hours to achieve a homogeneous mixture. Table 1 shows the key parameters that varied in the experiments.

Cases I and II were used to study particle migration, whereas Case III was used to obtain the velocity profiles in the straight and wavy microchannels. All the experiments were conducted in a pressure-driven flow configuration. Two flow rates were chosen such that the larger flow rate is approximately five times, the smaller one. The flow Reynolds numbers (Re) for the straight channel are about 10 and 50, corresponding to the two flow rates, and they are 8 and 38 for the wavy channel. After achieving a fully developed flow, the laser was fired to illuminate the solid particles through the objective lens (volume illumination). A timing or trigger box was used to synchronize the camera and laser flashlight to capture clear pictures of particle behavior in the flow as they travel through the microchannel. The thickness of the viewing plane (laser sheet) is approximately 5 µm. A long-pass optical filter was utilized to eliminate the reflected light from the microchannel walls.

In this study, the graphs of velocity and concentration profiles were reported mainly for two regions of the microchannel: inlet and outlet. The data were collected at 1.2 mm from the channel's inlet (i.e., after three sine waves) for the inlet profiles. Similarly, for the outlet profiles, the study window was positioned at 1.2 mm before the channel outlet. The very low concentrations of the particles shown in Table 1 were assumed not to affect the flow field.

Stokes–Einstein diffusion coefficient (D_{S-E} in Eq. (2)) was calculated for both particle sizes to verify the absence of Brownian motion (Castillo et al. 1994).

$$D_{S-E} = \frac{k_b \cdot T}{6\pi \cdot \mu \cdot R_0} \tag{2}$$

In Eq. (2), k_b is the Boltzmann constant (= 1.380×10^{-23} J/K), T is the temperature of the suspension in K, μ is the dynamic viscosity of the suspension, and R_0 is the particle radius. The temperature was assumed as 290 K based on the room temperature measurements during the experiments. The corresponding D_{S-E} for the 2 µm and 6 µm particles are 2.12×10^{-13} m²/s and 0.71×10^{-13} m²/s, respectively. These values are at least four orders of magnitude lower than the diffusion coefficients reported in prior studies on Brownian motion (e.g., Table 1 in ref. (Castillo et al. 1994) and Table 2 in ref. (Ould-Kaddour and Levesque 2000)). Therefore, Brownian motion was neglected in this study.

2.1 Uncertainty analysis

An uncertainty analysis was conducted to ensure that the sampled number of images was sufficient to yield consistent particle count results (or density or concentration) based on their spatial location. Seven hundred fifty pictures of the inlet and outlet windows were captured for both channel geometries, which served as the baseline. For
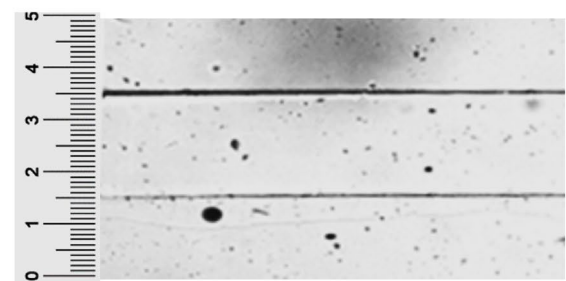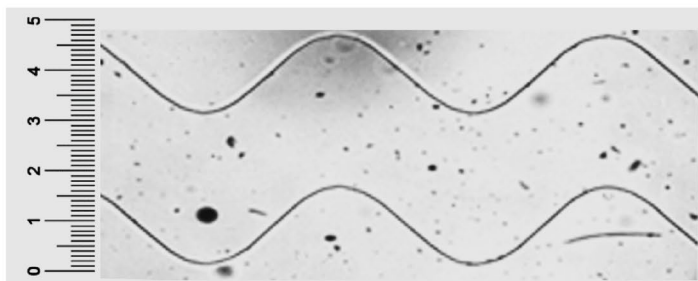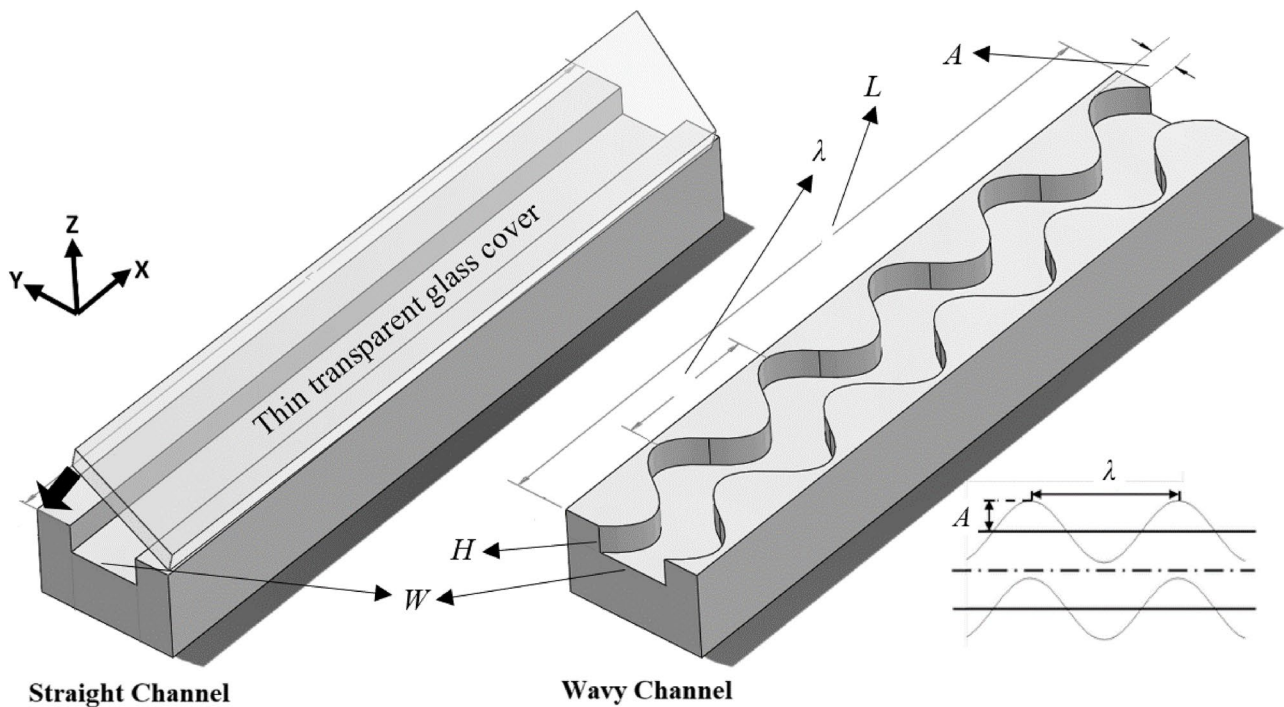
Fig. 2 Schematics of the microchannels (top) and the top view of their fabricated counterparts (bottom). A thin transparent glass cover was used to seal and confine the flow in the microchannels and enabled visualization of the flow

Table 1 Parameters varied in the experiments for studying the effect of engineered wall waviness on particle migration

	Particle size (μm)	Volumetric flow rate (μL/min)	Volume concentration
Case I	2	77 & 384	0.095% for the particle migration study
Case II	6	77 & 384	0.130% for the particle migration study
Case III	0.5	77 & 384	~0.0007% as appropriate for μ-PIV measurements for obtaining the velocity profiles

a sample size of 400 images, the uncertainty in the particle count in the straight channel flow was found to be ~3.5% on average, whereas, for the wavy channel, it was ~2.4%. Table 2 lists the uncertainties for both the channels at their inlet and outlet locations.

Table 2 Spatial uncertainty in the identification of particle locations in the captured images

	Straight channel	Wavy channel
Inlet	3.79%	2.61%
Outlet	3.11%	2.12%

2.2 Image processing algorithm

A MATLAB program was developed to process the images obtained using the μ-PIV setup, identify the particles, count the particles, and upload the data to a spreadsheet. The flow diagram of the algorithm for this program is shown in Fig. 3.

In the first step of the algorithm—while establishing the boundary regions for the channels—it was necessary to implement transformation matrices to rotate the coordinates of the straight line or the sinusoidal curve to account for a possible misalignment, if any, between the microfluidic device and the view plane of the camera. After establishing the boundaries for each section of the microchannel across its cross-section, a pixel intensity threshold was set for the entire channel to eliminate the out-of-focus particles, usually dimmer than the particles in focus. The process was repeated for all the images recognizing that the lighting conditions could vary depending on the location of the channel with respect to the laser source and the camera.

Next, images were cropped to fit a study window of 200 μm × 100 μm for the straight channel and 375 μm × 100 μm for the wavy channel. The study window was later divided into 12 equal-sized grids or bins for the straight channel and 15 grids or bins for the sinusoidal wavy channel. Figure 4 shows the bins for both channels. It also indicates bins 4–15 marking the wavy channel width.
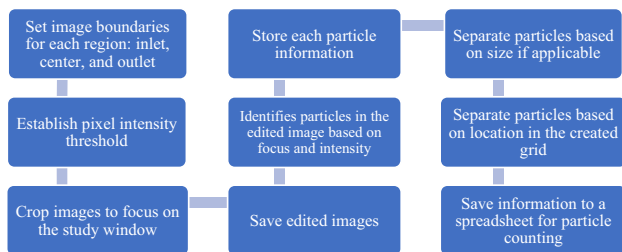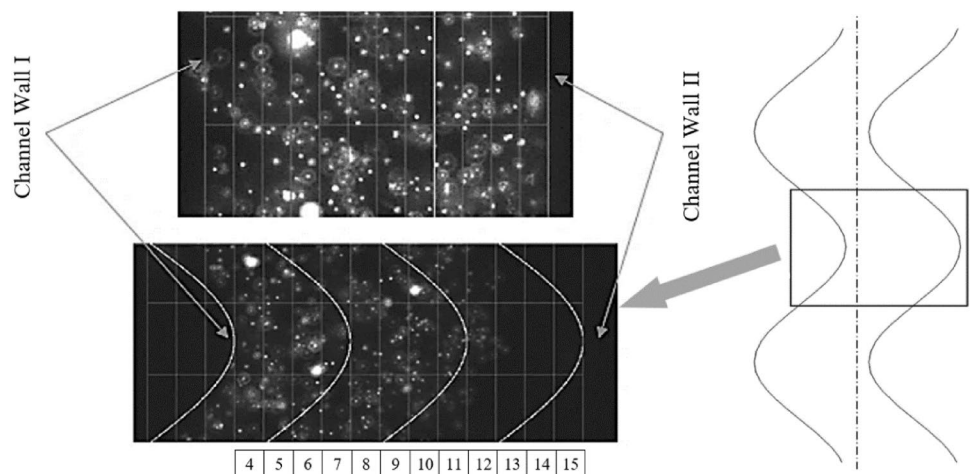
Within the bins, the particles were identified based on their circumference, and each particle was assigned a distinct tag. The algorithm then gathered individual particle information such as area, diameter, intensity, and centroid in the X and Y axes. The procedure was repeated for all the images, and the data were stored in a variable. The average results were then saved in a spreadsheet along with the data on individual regions in the grid. Figure 5 shows the critical steps in this regard.

A micro-scale ruler was used to calibrate the pixel scale to a micrometer scale. Then, based on the calibration parameter, the pixel thresholds for 2 μm and 6 μm particles were decided. Finally, the particle size was calculated using particle sample images and the thresholds.

3 Results and discussion

The particle concentration profiles in the straight and the wavy microchannels are displayed in Fig. 6 at the inlet and the outlet locations (described in Sect. 2) for particle sizes and the flow Re. In addition, the figure shows the bins (Sect. 2.2) for the microchannels and the concentration plots mapped over the vertical lines in the chart area corresponding to the bins.

Though the concentration profiles for the straight and wavy channels are shown in the same plot for ease of presentation, it must be noted that the size of bins is different between them due to the difference in their respective widths. A surfactant was added in the experiments (Sect. 2) to avoid actual particle agglomeration. Yet, particles close to each other appeared to accumulate at a few spatial locations. For these particles, variation of light along the depth of the laser sheet was found to be the reason for this appearance.
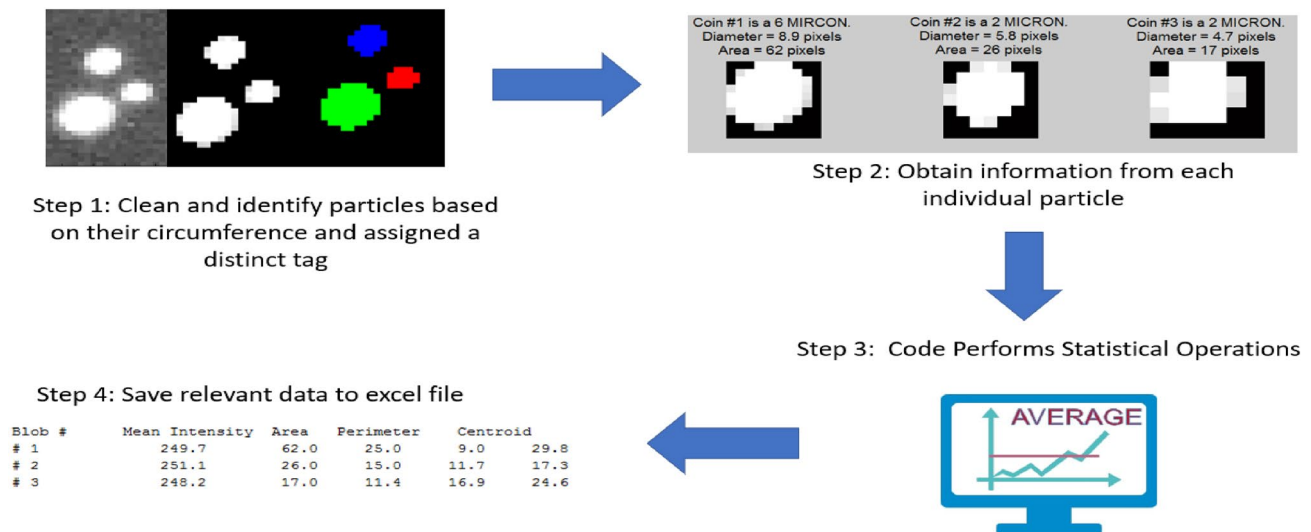
Salient observations from this figure are as follows.

Fig. 3 Particle counting algorithm

Fig. 4 Width of the microchannels established between the boundaries, Channel Wall I to the left and Channel Wall II to the right. The flow is in the vertical direction in the figure

Fig. 5 Particle identification and counting modules of the algorithm

1. The profiles are not smooth due to the very dilute concentration of the suspensions. Furthermore, the concentration in the images is further diluted due to capturing them in a 5-µm-thick plane (laser sheet thickness) in the height direction at H/2 from the above (Fig. 2). Therefore, a high-fidelity image processing algorithm and an uncertainty analysis with hundreds of images were pursued to handle the very low concentration (Sec. 2.2).

2. The particle migration where it occurred is shear-induced.

3. The concentration profiles in the straight channel do not show a noticeable variation between the inlet and the outlet. The variations mainly were within the experimental uncertainties (except close to the walls).

4. Relative to the straight channel, the concentration profiles in the wavy channel show a variation between the inlet and the outlet, even when including the experimental uncertainties and the fact that its width, W (of the migration plane), is 1.5 times larger than the straight channel. In other words, it is known that the shear gradient will be smaller in wider channels, yet the particle migration is more notable in the wavy channels.

5. The concentration profiles seem to migrate and settle into two streams at the outlet of the wavy microchannel, e.g., in and near bins 4 and 5 and 10 and 11. This settling occurs because bins 4 and 5 are closer to the wave crest (on Channel Wall I in Fig. 4) in the image-capturing window, while bins 10 and 11 are closer to the previous wave crest (on Channel Wall II in Fig. 4) that is spatially located before the flow enters the imaging window.

6. Consistent with the theory, the settling of the particles into two streams—one near each wall—in the wavy microchannel appears to be more pronounced for larger particles (here, 6 µm) and higher flow Re (here, 38) based on the particle percentages shown on the y-axis.

These observations are discussed in detail in the subsequent paragraphs.

The migration mechanism was determined based on the particle Reynolds number (Re_p), shown in Eqs. (3) and (4) (Carlo et al. 2007).

$$Re_p = Re_c \cdot \frac{d_p^2}{D_h^2} \tag{3}$$

In Eq. (3), D_h ($= 2 \bullet W \cdot H/(W + H)$) is the microchannel's hydraulic diameter, and Re_c is the channel Reynolds number based on the maximum velocity of the fluid (U_m) and is given by:
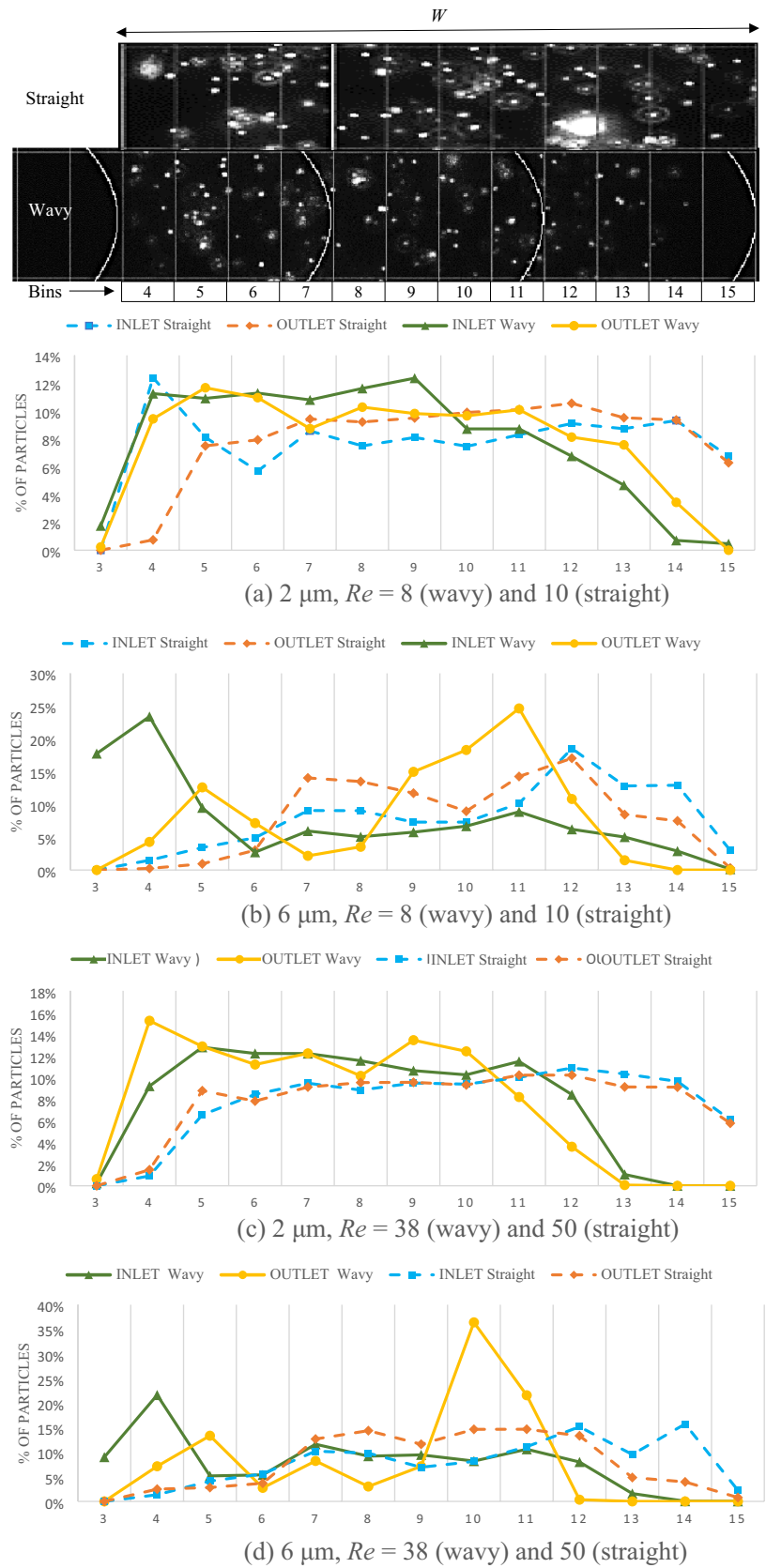
$$Re_c = \frac{\rho \cdot U_m \cdot D_h}{\mu} \tag{4}$$

In Eq. (4), ρ is the density of the suspension, and μ is its absolute viscosity. A reasonable value of U_m for the suspension flow can be estimated from mass continuity using ρ, the flow rates (shown in Table 1), and the microchannel cross-sectional area (W X H). The absolute viscosity was obtained using Eq. (5) for diluted suspensions of concentrations less than 2% (Einstein 1906).

$$\mu = \mu_{water} \cdot (1 + 2.5 \cdot c) \tag{5}$$

where μ_{water} is the absolute viscosity of water and c is the particle concentration ($= 0.1\%$).

Fig. 6 Concentration profiles obtained from flow visualization in straight and wavy microchannels for the flow of very dilute suspensions (~0.1% volume concentration) at flow Re < 100
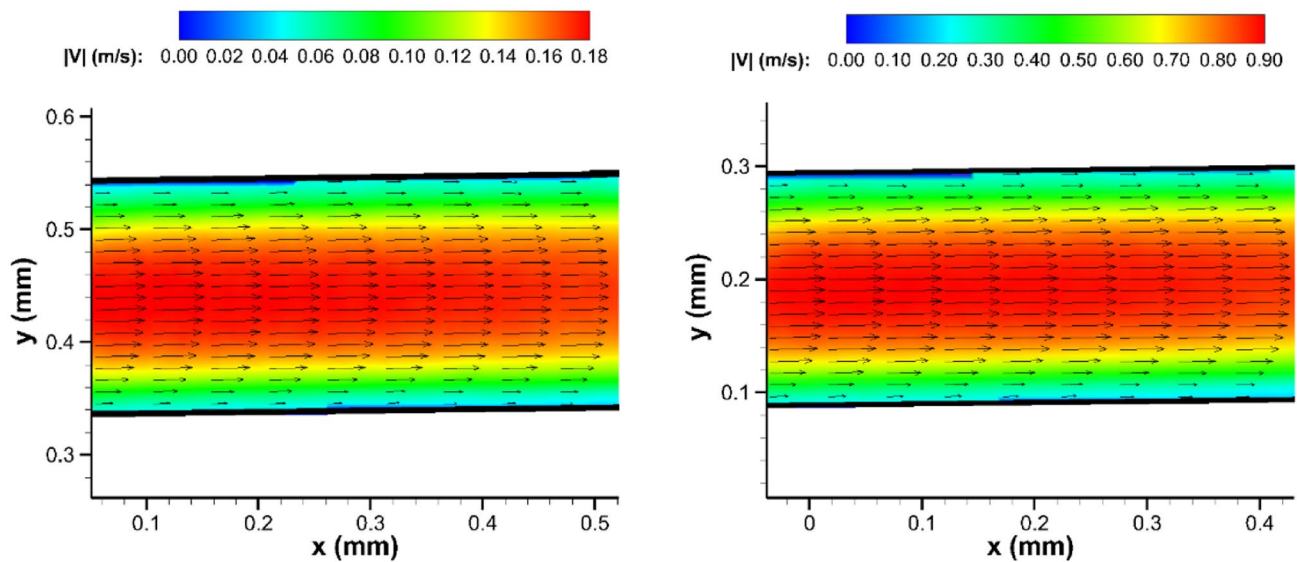

(a) 2 μm, $Re = 8$ (wavy) and 10 (straight)

(b) 6 μm, $Re = 8$ (wavy) and 10 (straight)

(c) 2 μm, $Re = 38$ (wavy) and 50 (straight)

(d) 6 μm, $Re = 38$ (wavy) and 50 (straight)

Fig. 7 Velocity contours in the straight microchannel for Re = 10 (left) and 50 (right) as measured by the μ-PIV system

From Eq. (3), Re_p was found to be 0.023 and 0.210 for the 2 μm and the 6 μm particles, respectively, for the flow through the straight channel for the larger Re of 50. For the wavy channel, the corresponding values were 0.014 and 0.127, respectively, for the larger Re of 38. Since Re_p is less than 1 for all the cases, the mode of particle migration can be assumed as predominantly shear-induced.

The third observation (for the straight channel) aligns with the theory of shear-induced migration for very dilute suspensions. The concentration distribution is the same at the inlet, along the length, and at the outlet of the microchannel.

The migration length (L_m) required to attain the equilibrium position—which is near the center of the microchannel for shear-induced migration—in the plane of observation (width, W) can be approximately estimated using Eq. (6) (Leighton and Acrivos 1987; Nott and Brady 1994). A highly conservative diffusion coefficient, $d(\varphi)$, of 0.1 was assumed, which applies to 25% concentration suspensions. For a very dilute 0.1% suspension, the d(φ) value will be significantly smaller than 0.1.

$$L_m = \frac{W^3}{12 \cdot d(\varphi) \cdot d_p^{\,2}} \tag{6}$$

The values of L_m for the 2 μm and the 6 μm particles were estimated as ~ 167 cm and ~ 19 cm, respectively. Considering the microchannel length in the present study is 6 cm, it is concluded that the particle migration phenomenon is only in the initial stages in the straight channel ($W = 200$ μm) at its outlet.

If Eq. (6) is assumed to be reasonable for obtaining a rough estimate of L_m for the wavy microchannel ($W = 300$ μm), its values for the 2 μm and the 6 μm particles will be ~ 562 cm and ~ 63 cm, respectively. However, relative to the straight channel, concentration profiles in the wavy channel were observed to show a variation between the inlet and the outlet. In the plane of view under consideration, high concentrations of particles were observed near the wave peaks or crests in the 6 cm effective microchannel length, which is only ~ 1% and ~ 10% of the L_m, respectively, for the two particle sizes. This rapid migration phenomenon of the particles toward walls in the wavy microchannel can be explained by discussing the flow velocity profiles.

The μ-PIV results for the flow through a straight microchannel are shown in Figs. 7 and 8. For both the tested flow rates, it can be observed that the velocity profile across the channel width is symmetrically parabolic in agreement with the theory (which could be considered a validation of the test setup).

For example, for a two-dimensional flow scenario through the straight-walled channel—such as between two parallel plates separated by a width W—the symmetrically parabolic velocity profile is given by Eq. (7).

$$u(y) = \frac{G}{2\mu} \cdot [y] \cdot [y - W] \tag{7}$$

In Eq. (7), y is the spatial variable in the width direction (as described in Eq. (1)) and $G = -(dP/dy)$, the pressure gradient. For Eq. (7), the magnitude of the wall shear stress ($\tau_{w,straight}$) can be shown to be equal on either of the two walls (and perfectly symmetrical) in the straight-walled microchannel (Eqs. (8) and (9)).
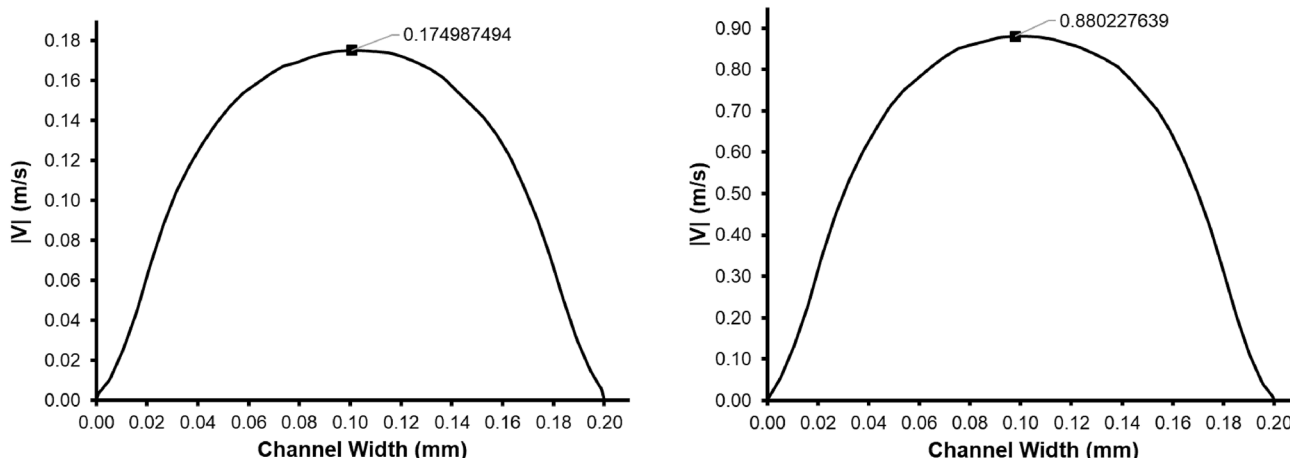
Fig. 8 Post-processed velocity profiles in the straight microchannel for Re = 10 (left) and 50 (right)

$$\tau_w = \mu \cdot \left[\frac{du}{dy}\right]_{y=0} \tag{8}$$

$$\left|\tau_{w,straight}\right| = \frac{G}{2} \cdot W \tag{9}$$

The velocity field in the wavy microchannel is shown in Fig. 9 and noted to be different from that in the straight microchannel. It was asymmetric, with the high-velocity region alternately concentrated near the peaks of the two wavy walls, as shown in Fig. 10. In Fig. 11, plotting the velocity profile from the μ-PIV data when the wave crest is on Channel Wall I showed the maximum velocity to occur near this wall (Fig. 11b, angle $\varphi = \pi/2$). Similarly, plotting the velocity profile when the wave crest is on Channel Wall II showed the maximum velocity to occur near this wall (Fig. 11d, $\varphi = 3\pi/2$).

Based on these results, it is concluded that the velocity profile oscillates between the two wavy walls while the fluid flows through the microchannel, and the sine curve's shape governs this oscillation. The velocity profile was approximately symmetric between the crest and the trough regions of any one wavy wall (Fig. 11c, $\varphi = \pi$).

The asymmetric velocity profile in the wavy channel can also be understood by developing a simple analytical solution for the two-dimensional flow case of a fluid akin to the parallel plate flow theory discussed for the straight channel. In this case, the boundary conditions and the velocity profile for such a pressure-driven flow through two wavy parallel plates can be shown to follow Eqs. (10)-(13).

$$\mu \frac{\partial^2 u}{\partial y^2} = \frac{\partial p}{\partial x} \tag{10}$$

$$u = 0 \text{ at } y = A \cdot \sin\left(\frac{2\pi}{\lambda}x\right) \tag{11}$$

$$u = 0 \text{ at } y = A \cdot \sin\left(\frac{2\pi}{\lambda}x\right) + W \tag{12}$$

$$u(y) = \frac{G}{2\mu} \cdot \left[y - A \cdot \sin\left(\frac{2\pi}{\lambda}x\right)\right] \cdot \left[y - A \cdot \sin\left(\frac{2\pi}{\lambda}x\right) - W\right] \tag{13}$$

It can be shown from Eq. (13) that this asymmetric velocity profile creates an asymmetric wall shear stress ($\tau_{w,wavy}$) for the wavy channel. The magnitude of $\tau_{w,wavy}$ varies in the lateral direction between a trough on one wavy wall and a crest on the opposite wavy wall, as shown in Eq. (14).

$$\frac{G}{2} \cdot \left(W - 2 \cdot A \cdot \sin\left(\frac{2\pi}{\lambda}x\right)\right) \le \left|\tau_{w,wavy}\right| \le \frac{G}{2} \cdot \left(W + 2 \cdot A \cdot \sin\left(\frac{2\pi}{\lambda}x\right)\right) \tag{14}$$

This variation in $\tau_{w,wavy}$ could be particularly significant (e.g., an order of magnitude difference between the values at the two opposite walls) if the amplitude and the wavelength of the sine wave are comparable to the channel size. As a reminder, W (= 300 μm), A (= 80 μm), and λ (= 400 μm) are comparable in the present study. A considerable variation in $\tau_{w,wavy}$ in the lateral direction, induces a large shear stress gradient in the fluid. This large gradient is postulated to move the particles toward the maximum velocity region (i.e., closer to the wave crests) where the shear stress is a minimum (the smallest slope of the curve in Figs. 10 and 11).

Furthermore, from Fig. 11, it can be observed that the maximum velocity in the wavy microchannel for $Re = 38$ decreases from ~0.9175 m/s to ~0.8856 m/s when the fluid moves from φ of $\pi/2$ to π, and it increases again to ~0.9190 m/s when flow approaches a φ of $3\pi/2$. While
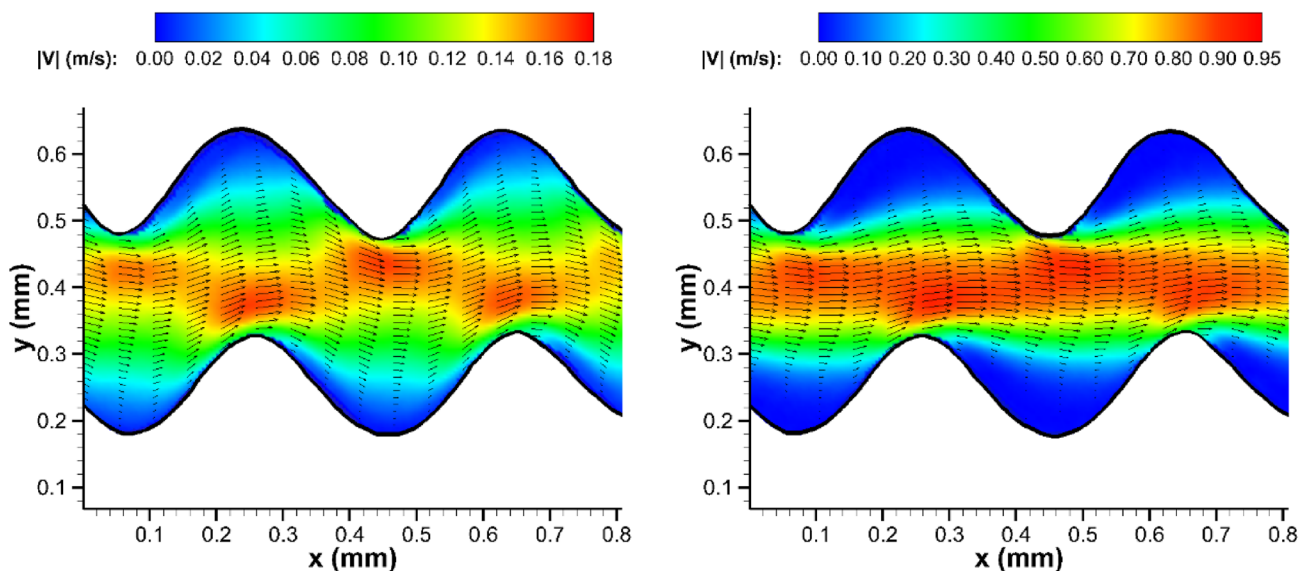
Fig. 9 Velocity contours in the wavy microchannel for Re = 8 (left) and 38 (right) as measured by the μ-PIV system
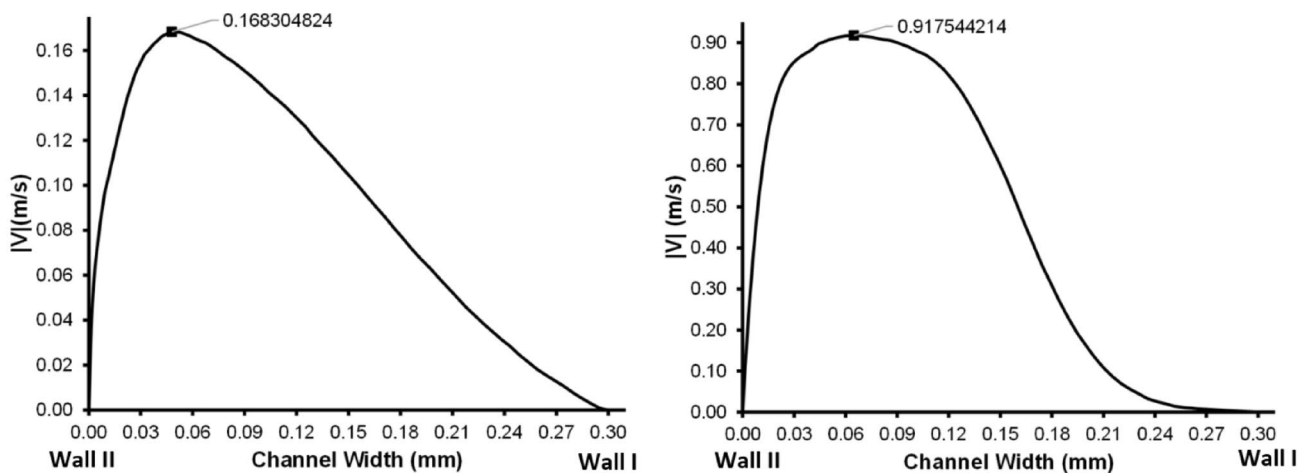

Fig. 10 Post-processed velocity profiles in the wavy microchannel (local values shown as V on the y-axis) for Re = 8 (left) and 38 (right) at an angle of π/2 for the sine wave

the maximum velocity remains a constant at the centerline for the fully developed flow through a straight channel, this change in its magnitude—specifically the increase near the wave crests—in the wavy channel alludes to a flow-squeezing effect in the latter. This effect is expected to create a more significant variation in the local velocity field and the associated shear gradients. Due to this converging–diverging flow effect produced by the wavy

microchannels, they might also be considered for controlling the particle alignment in suspensions of anisotropic particles with shapes such as ellipsoids or rods, e.g., carbon nanotubes and fibrous proteins and cells (Oumer and Mamat 2013; Trebbin et al. 2013; Siqueira et al. 2017b).

Particle migration is considerably slow compared to the rapidly changing velocity profile alternating between the two walls in the wavy microchannel. Hence, it is hypothesized that once particles attain the lowest shear stress
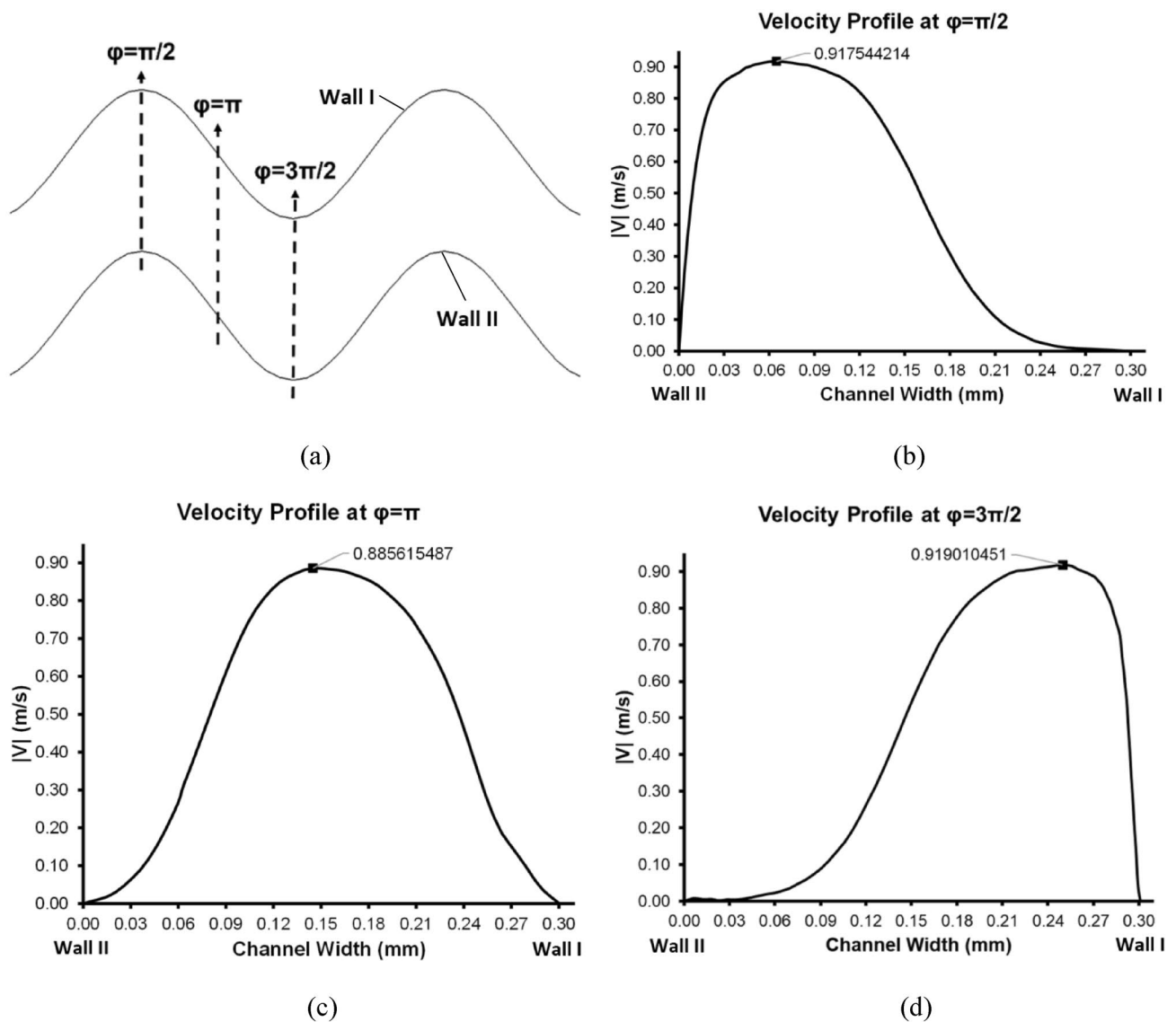
Fig. 11 Velocity profiles for the flow through the sinusoidal wavy microchannel (local values shown as V on the y-axis) at different locations on the wave along the flow length for a flow Re of 38

position closer to the wave crest of a wall, they follow the same path between any two crests of that wall (vs. oscillating between the two walls). This hypothesis implies that particles in the flow will align into two streams, one near each wavy wall. This phenomenon could be conveniently used for achieving their separation, sorting, or filtration in many chemical and biological applications. This hypothesis was supported by the instantaneous images of the suspension flow captured using the μ-PIV setup, especially for the 6 μm particles (Fig. 12) that migrated or settled faster than the 2 μm particles.

Of note from the results of the μ-PIV measurements of the velocity profiles is the absence of secondary flows in the wavy microchannel for achieving the observed particle migration (Figs. 9–11). This aspect contrasts with the passive approaches that use channel curvature (e.g., spiral channels) to generate secondary flows and a resulting additional drag force to aid in the particle migration, but which also increases the pressure drop required for moving the suspension through the microchannel. As a theoretical basis for this note—for the cases pursued in this study—the Dean
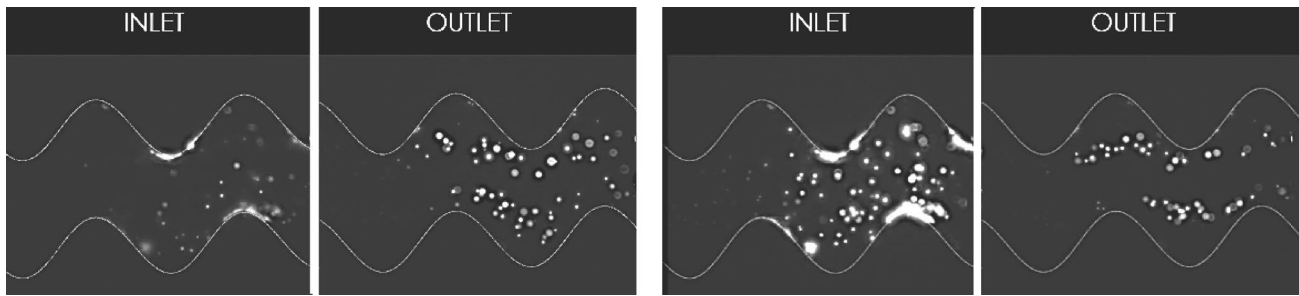
Fig. 12 Instantaneous μ-PIV images showing particle migration in the flow toward wave crests and the presence of two particle streams, one near each wavy wall, for Re = 8 (left) and 38 (right). The flow is in the horizontal direction from left to right

number (*De*) was calculated. It was found to be 11, and 53 for the two flow rates sought in this study, implying a lack of secondary flow due to the wall waviness.

4 Conclusions

In this effort, two-dimensional waviness was assigned to the walls of a confined microchannel. Flow visualization was employed to study whether this passive approach could influence the shear-induced migration phenomenon in a very dilute suspension (0.1% concentration) for flow Reynolds numbers less than 100. The approach was tested for two different particle sizes (2 μm and 6 μm) and two flow rates in a pressure-driven flow configuration. The following notes and conclusions are drawn from this study.

1. For the straight microchannel, the concentration profiles did not show a noticeable variation between the inlet and the outlet locations, in line with the theory of shear-induced migration of very dilute suspensions.
2. Relative to the straight microchannel, the concentration profiles in the wavy microchannel—that is 1.5 times wider than the straight microchannel—showed that the migration process has started to stabilize for a substantially smaller effective microchannel length than the theoretical length required for the particles to occupy an equilibrium position in a straight microchannel.
3. For the wavy microchannel, the concentration profiles appear to settle into two streams at the outlet, one near each wall. These two streams were found to be closer to the wave crests of the walls and follow the same path between any two crests of one wall. This unique migration phenomenon can be conveniently used for particle separation, sorting, or filtration in many chemical, biological, and biomedicine applications.
4. Of particular note is that the observed particle migration in the wavy microchannel was achieved without secondary flows that typically cause an increase in the pressure drop or the pumping power requirement.

5. Due to the converging-diverging flow effect produced by the wavy microchannels, they might also be considered for controlling the particle alignment in suspensions of anisotropic particles with shapes such as ellipsoids or rods, e.g., carbon nanotubes and fibrous proteins and cells.

Declarations

Conflict of interests The authors declare no competing interests.

References

Alshareef M, Metrakos N, Juarez Perez E, Azer F, Yang F, Yang X, Wang G (2013) Separation of tumor cells with dielectrophoresis-based microfluidic chip. Biomicrofluidics 7(1):011803. https://doi.org/10.1063/1.4774312

Ateya DA, Erickson JS, Howell PB, Hilliard LR, Golden JP, Ligler FS (2008) The good, the bad, and the tiny: a review of microflow cytometry. Anal Bioanal Chem 391(5):1485–1498

Bhagat AAS, Bow H, Hou HW, Tan SJ, Han J, Lim CT (2010) Microfluidics for cell separation. Med Biol Eng Compu 48(10):999–1014

Boyer F, Guazzelli É, Pouliquen O (2011) Unifying suspension and granular rheology. Phys Rev Lett 107(18):188301

Callow JA, Callow ME (2011) Trends in the development of environmentally friendly fouling-resistant marine coatings. Nat Commun 2(1):1–10

Castillo R, Garza C, Ramos S (1994) Brownian motion at the molecular level in liquid solutions of C60. J Phys Chem 98(15):4188–4190

Conkey DB, Trivedi RP, Pavani SRP, Smalyukh II, Piestun R (2011) Three-dimensional parallel particle manipulation and tracking by integrating holographic optical tweezers and engineered point spread functions. Opt Express 19(5):3835–3842

Cunha FR, Rosa AP, Dias NJ (2016) Rheology of a very dilute magnetic suspension with micro-structures of nanoparticles. J Magn Magn Mater 397:266–274

Davis RH, (2019) Microfiltration in pharmaceutics and biotechnology. Curr Trends Future Dev (Bio-) Membranes, pp 29–67

Dbouk T, Habchi C (2019) On the mixing enhancement in concentrated non-colloidal neutrally buoyant suspensions of rigid particles using helical coiled and chaotic twisted pipes: a numerical investigation. Chem Eng Process-Process Intens 141:107540

Di Carlo D, Irimia D, Tompkins RG, Toner M (2007) Continuous inertial focusing, ordering, and separation of particles in microchannels. Proc Natl Acad Sci 104(48):18892–18897

Dontsov EV, Boronin SA, Osiptsov AA, Derbyshev DY (2019) Lubrication model of suspension flow in a hydraulic fracture with frictional rheology for shear-induced migration and jamming. Proc R Soc A 475(2226):20190039

Einstein A (1906) A new analysis of molecule dimensions. Ann Phys 19:289–306

Esseling M, Glasener S, Volonteri F, Denz C (2012) Opto-electric particle manipulation on a bismuth silicon oxide crystal. Appl Phys Lett 100(16):161903

Fan X, Phan-Thien N, Yong NT, Wu X, Xu D (2003) Microchannel flow of a macromolecular suspension. Phys Fluids 15(1):11–21

Gadala-Maria F, Acrivos A (1980) Shear-induced structure in a concentrated suspension of solid spheres. J Rheol 24(6):799–814

Gallager SM (1988) Visual observations of particle manipulation during feeding in larvae of a bivalve mollusc. Bull Mar Sci 43(3):344–365

Gao Y (2017) Inertial migration of particles in microchannel flows. Doctoral dissertation, INSA de Toulouse

Goris S, Osswald TA (2018) Process-induced fiber matrix separation in long fiber-reinforced thermoplastics. Compos A Appl Sci Manuf 105:321–333

Guan G, Wu L, Bhagat AA, Li Z, Chen PCY, Chao S, Ong CJ, Han J (2013) Spiral microchannel with rectangular and trapezoidal cross-sections for size based particle separation. Sci Rep 3(1):1–9

Hampton RE, Mammoli AA, Graham AL, Tetlow N, Altobelli SA (1997) Migration of particles undergoing pressure-driven flow in a circular conduit. J Rheol 41(3):621–640

Hardt S, Schönfeld F (2007) Microfluidic technologies for miniaturized analysis systems. Springer Science & Business Media, New York

Hong CM, Kim J, Jana SC (2004) Shear-induced migration of conductive fillers in injection molding. Polym Eng Sci 44(11):2101–2109

Jonáš A, Zemanek P (2008) Light at work: the use of optical forces for particle manipulation, sorting, and analysis. Electrophoresis 29(24):4813–4851

Kang L, Chung BG, Langer R, Khademhosseini A (2008) Microfluidics for drug discovery and development: from target selection to product lifecycle management. Drug Discovery Today 13(1–2):1–13

Karimi A, Yazdi S, Ardekani AM (2013) Hydrodynamic mechanisms of cell and particle trapping in microfluidics. Biomicrofluidics 7(2):021501

Karnis, 2., Goldsmith, H.L. and Mason, S.G., (1966) The kinetics of flowing dispersions: I. Concentrated suspensions of rigid particles. J Colloid Interface Sci 22(6): 531–553

Kiyasatfar M, Nama N (2018) Particle manipulation via integration of electroosmotic flow of power-law fluids with standing surface acoustic waves (SSAW). Wave Motion 80:20–36

Klaver RM, Schroën CGPH (2015) A review of shear-induced particle migration for enhanced filtration and fractionation. Modeling Food Processing Operations 211–233. https://doi.org/10.1016/B978-1-78242-284-6.00008-8

Koh CJ, Hookham P, Leal LG (1994) An experimental investigation of concentrated suspension flows in a rectangular channel. J Fluid Mech 266:1–32

Kumar D, Shenoy A, Deutsch J, Schroeder CM (2020) Automation and flow control for particle manipulation. Curr Opin Chem Eng 29:1–8

Kuravi S (2009) Numerical study of encapsulated phase change material (EPCM) slurry flow in microchannels. Doctoral dissertation, University of Central Florida

Kuravi, S., Kota, K.M., Du, J. and Chow, L.C., 2009. Numerical investigation of flow and heat transfer performance of nano-encapsulated phase change material slurry in microchannels. J Heat Trans, 131(6)

Lee CY, Chang CL, Wang YN, Fu LM (2011) Microfluidic mixing: a review. Int J Mol Sci 12(5):3263–3287

Leighton D, Acrivos A (1987) The shear-induced migration of particles in concentrated suspensions. J Fluid Mech 181:415–439

Li S, Li M, Bougot-Robin K, Cao W, Yeung Yeung Chau I, Li W, Wen W (2013) High-throughput particle manipulation by hydrodynamic, electrokinetic, and dielectrophoretic effects in an integrated microfluidic chip. Biomicrofluidics 7(2):024106. https://doi.org/10.1063/1.4795856

Liu C, Hu G (2017) High-throughput particle manipulation based on hydrodynamic effects in microchannels. Micromachines 8(3):73. https://doi.org/10.3390/mi8030073

Martel JM, Toner M (2014) Inertial focusing in microfluidics. Annu Rev Biomed Eng 16:371. https://doi.org/10.1146/annurev-bioeng-121813-120704

Mirowski E, Moreland J, Russek SE, Donahue MJ (2004) Integrated microfluidic isolation platform for magnetic particle manipulation in biological systems. Appl Phys Lett 84(10):1786–1788

Morris JF, Boulay F (1999) Curvilinear flows of noncolloidal suspensions: the role of normal stresses. J Rheol 43(5):1213–1237

Nguyen NT, Shaegh SAM, Kashaninejad N, Phan DT (2013) Design, fabrication and characterization of drug delivery systems based on lab-on-a-chip technology. Adv Drug Deliv Rev 65(11–12):1403–1419

Nilsson J, Evander M, Hammarström B, Laurell T (2009) Review of cell and particle trapping in microfluidic systems. Anal Chim Acta 649(2):141–157

Nir S, Reches M (2016) Bio-inspired antifouling approaches: the quest towards non-toxic and non-biocidal materials. Curr Opin Biotechnol 39:48–55

Niu F, Ma W, Li X, Chu HK, Yang J, Ji H, Sun D (2014) Modeling and development of a magnetically actuated system for micro-particle manipulation.14th IEEE International Conference on Nanotechnology 127–130. https://doi.org/10.1109/NANO.2014.6967976

Nott PR, Brady JF (1994) Pressure-driven flow of suspensions: simulation and theory. J Fluid Mech 275:157–199

Ould-Kaddour F, Levesque D (2000) Molecular-dynamics investigation of tracer diffusion in a simple liquid: test of the Stokes-Einstein law. Phys Rev E 63(1):011205

Oumer AN, Mamat O (2013) A review of effects of molding methods, mold thickness and other processing parameters on fiber orientation in polymer composites. Asian J Sci Res 6(3):401

Paiè P, Zandrini T, Vázquez RM, Osellame R, Bragheri F (2018) Particle manipulation by optical forces in microfluidic devices. Micromachines 9(5):200. https://doi.org/10.3390/mi9050200

Petrie CJ (1999) The rheology of fibre suspensions. J Nonnewton Fluid Mech 87(2–3):369–402

Phillips RJ, Armstrong RC, Brown RA, Graham AL, Abbott JR (1992) A constitutive equation for concentrated suspensions that accounts for shear-induced particle migration. Phys Fluids A 4(1):30–40

Rebouças RB, Siqueira IR, Carvalho MS (2018) Slot coating flow of particle suspensions: particle migration in shear sensitive liquids. J Nonnewton Fluid Mech 258:22–31

Ren Q, Liang C (2020) Insulator-based dielectrophoretic antifouling of nanoporous membrane for high conductive water desalination. Desalination 482:114410

Said KAM, Ismail AF, Karim ZA, Abdullah MS, Usman J, Raji YO (2020) Innovation in membrane fabrication: magnetic induced photocatalytic membrane. J Taiwan Inst Chem Eng 113:372–395

Schroen K, van Dinther A, Stockmann R (2017) Particle migration in laminar shear fields: a new basis for large scale separation technology? Sep Purif Technol 174:372–388

Segre G, Silberberg A (1962) Behaviour of macroscopic rigid spheres in Poiseuille flow Part 2. Experimental results and interpretation. Journal of fluid mechanics, 14(1):136–157. https://doi.org/10.1017/S0022112062001111

Siqueira IR, Carvalho MS (2019) A computational study of the effect of particle migration on the low-flow limit in slot coating of particle suspensions. J Coat Technol Res 16(6):1619–1628

Siqueira IR, Rebouças RB, Carvalho MS (2017a) Particle migration and alignment in slot coating flows of elongated particle suspensions. AIChE J 63(7):3187–3198

Siqueira IR, Rebouças RB, Carvalho MS (2017b) Migration and alignment in the flow of elongated particle suspensions through a converging-diverging channel. J Nonnewton Fluid Mech 243:56–63

Solehati N, Bae J, Sasmito AP (2018) Optimization of wavy-channel micromixer geometry using Taguchi method. Micromachines 9(2):70

Suresh S, Spatz J, Mills JP, Micoulet A, Dao M, Lim CT, Beil M, Seufferlein T (2005) Connections between single-cell biomechanics and human disease states: gastrointestinal cancer and malaria. Acta Biomater 1(1):15–30

Trebbin M, Steinhauser D, Perlich J, Buffet A, Roth SV, Zimmermann W, Thiele J, Förster S (2013) Anisotropic particles align perpendicular to the flow direction in narrow microchannels. Proc Natl Acad Sci 110(17):6706–6711

Tripathi D, Bég OA (2014) A study on peristaltic flow of nanofluids: application in drug delivery systems. Int J Heat Mass Transf 70:61–70

Varanakkottu SN, George SD, Baier T, Hardt S, Ewald M, Biesalski M (2013) Particle manipulation based on optically controlled free surface hydrodynamics. Angew Chem Int Ed 52(28):7291–7295. https://doi.org/10.1002/anie.201302111

Vaziri A, Gopinath A (2008) Cell and biomolecular mechanics in silico. Nat Mater 7(1):15–23

Wang H, Qiu Y, Demore C, Cochran S, Glynne-Jones P, Hill M (2012) Particle manipulation in a microfluidic channel with an electronically controlled linear piezoelectric array. IEEE International Ultrasonics Symposium 2012:1–4. https://doi.org/10.1109/ULTSYM.2012.0500

Xie C, Chen B, Yan B, Wu J (2018) A new method for particle manipulation by combination of dielectrophoresis and field-modulated electroosmotic vortex. Appl Math Mech 39(3):409–422

Yadav S, Reddy MM, Singh A (2015) Shear-induced particle migration in three-dimensional bifurcation channel. Int J Multiph Flow 76:1–12

Zhang S, Wang Y, Onck P, den Toonder J (2020) A concise review of microfluidic particle manipulation methods. Microfluid Nanofluid 24(4):1–20. https://doi.org/10.1007/s10404-020-2328-5

Zhou Y, Ma Z, Ai Y (2018) Sheathless inertial cell focusing and sorting with serial reverse wavy channel structures. Microsyst Nanoeng 4(1):1–14